https://doi.org/10.5194/hess-2021-50
Preprint. Discussion started: 23 February 2021

Hydrology and Earth System Sciences
Open Access
Discussions

Evaluation of hillslope storage with variable width under temporally varied rainfall recharge

Ping-Cheng Hsieh[1] and Tzu-Ting Huang[2]

[1] Department of Soil and Water Conservation, National Chung Hsing University, Taichung 40227, Taiwan.

[2] Department of Water Resources, Taoyuan City Government, Taoyuan 330, Taiwan.

*Corresponding author: Ping-Cheng Hsieh (pchsieh@nchu.edu.tw; ida364@email.nchu.edu.tw)

https://doi.org/10.5194/hess-2021-50
Preprint. Discussion started: 23 February 2021

Hydrology and Earth System Sciences
Discussions

Abstract. This study discussed water storage in aquifers of hillslopes under temporally varied rainfall recharge by employing a hillslope-storage equation to simulate groundwater flow. The hillslope width was assumed to vary exponentially to denote the following complex hillslope types: uniform, convergent, and divergent. Both analytical and numerical solutions were acquired for the storage equation with a recharge source. The analytical solution was obtained using an integral transform technique. The numerical solution was obtained using a finite difference method in which the upwind scheme was used for space derivatives and the third-order Runge–Kutta scheme was used for time discretization. The results revealed that hillslope type significantly influences the drains of hillslope storage. Drainage was the fastest for divergent hillslopes and the slowest for convergent hillslopes. The results obtained from analytical solutions require the tuning of a fitting parameter to better describe the groundwater flow. However, a gap existed between the analytical and numerical solutions under the same scenario owing to the different versions of the hillslope-storage equation. The study findings implied that numerical solutions are superior to analytical solutions for the nonlinear hillslope-storage equation, whereas the analytical solutions are better for the linearized hillslope-storage equation. The findings thus can benefit research on and have application in soil and water conservation.

Keywords: Groundwater; Boussinesq equation; Hillslope storage; Complex hillslopes.

1 Introduction

Mountains in Taiwan are considerably high and steep, and the flow velocity of surface water and subsurface water is so high that it can cause severe soil erosion on hillslopes. Therefore, the management of catchment areas has become a crucial issue in Taiwan. Generally, hillslope form, water transportation, sediment transport, and aquifer structure are the main factors affecting catchment.

Some in-situ observations and experiments have investigated subsurface water flow problems. For example, Anderson and Burt (1978) adopted an automatic system to detect soil moisture content and found that it is significantly affected by topography. Mosley (1979) measured overland flow and subsurface flow in a forest watershed and found that the flow discharge in a river is greatly influenced by overland flow and subsurface flow and that the subsurface flow is considerably decreased on mild slopes. O'Loughlin (1986) presented a topographic analysis approach to predict the saturated zone of a watershed. McDonnell (1990) conducted an isotope study and reported that the speed of water flow permeability in an aquifer is affected by the slope in a watershed by means of isotope study. Genereux et al. (1993) used a chemical method to time

https://doi.org/10.5194/hess-2021-50
Preprint. Discussion started: 23 February 2021

water flow from different upstream regions to the outlet and concluded that the travel time of flow can be topographically determined in a watershed. Woods and Rowe (1996) also reported that subsurface flow discharge significantly varies with topography and environmental conditions. Subsequently, Woods et al. (1997) presented a new topographic index to predict the spatial pattern change in subsurface flow and saturated zone thickness based on the collected data.

By contrast, some researchers have studied subsurface flow by using analytical approaches and numerical methods. Childs (1971) first derived a generalized Boussinesq equation to delineate groundwater flow in a sloping aquifer. Evans (1979) presented a bivariate quadrature function to represent different topographic surfaces of catchments and further integrated terrain analysis and slope mapping. Brutsaert (1994) linearized the Boussinesq equation and analytically solved it to describe groundwater level. This solution provides a crucial framework to study slope features and their hydrological response. Fan and Bras (1998) substituted Darcy's law into the continuity equation of subsurface flow and derived an analytical solution by using the method of characteristics. On the basis of Evans (1979), Troch et al. (2002) presented nine hillslopes to represent the conventional hillslope types in hydrology and used the method of characteristics to analytically solve the hillslope-storage kinematic wave equation for subsurface flow. Troch et al. (2003) changed the variable h (water depth) in the Boussinesq equation to s (hill storage) and then solved many versions of the equation by linearizing and simplifying it, using the finite difference method to discretize the space and the multistep solver to deal with time. Later, Troch et al. (2004) employed an exponential form to describe the variation of hillslope width and substituted it into the linearized Boussinesq equation; then, they analytically solved the equation by using the Laplace transform and compared the results with numerical solutions for the nonlinear hill-storage equation with uniform rainfall recharge.

Taken together, all the aforementioned studies have indicated that geology has a considerable influence on groundwater flow, but most studies have considered only uniform rainfall recharge rates. Therefore, the present study employed the hill-storage Boussinesq equation of Troch et al. (2003, 2004) to delineate groundwater flow and water storage in hillslopes but used randomly distributed recharge rates to comply with natural rainfall recharge conditions. The present numerical solution for the nonlinear Boussinesq equation was obtained using the finite difference method. Discretization in space was performed using the central difference and upwind scheme, but discretization in time was performed using the third-order total variation diminishing (TVD) Runge–Kutta scheme. The present analytical solution to the linearized equation was acquired using the generalized integral transforms technique presented by Özisik (1968).

https://doi.org/10.5194/hess-2021-50
Preprint. Discussion started: 23 February 2021

2 Mathematical formulation

Figure 1 presents a schematic of an aquifer overlying an impermeable base with an inclined angle θ. The ground surface is vegetation free, and the sole drain of groundwater is an open channel at the outlet. The aquifer was assumed to be saturated, homogeneous, and isotropic, with a constant thickness and variable width.

2.1 Governing equation

The continuity equation for groundwater flow with rainfall recharge yields

$$\frac{\partial s}{\partial t} = -\frac{\partial Q}{\partial x} + Rw \tag{1}$$

where s is water storage [L^2], Q is discharge [L^{3}T^{-1}], w is the hillslope width function of the flow distance x [L], and R is rainfall recharge [LT^{-1}].

Because the hillslope width in this study is not constant, the equation of hillslope width proposed by Troch et al. (2004) was introduced to delineate three hillslope types: convergent, uniform, and divergent.

$$w(x) = ce^{ax} \tag{2}$$

where c is the width at the outlet [L] and a is a parameter [L^{-1}]. The hillslope type is convergent if $a > 0$, uniform if $a = 0$, and divergent if $a < 0$.

The flow discharge obeying Darcy's law yields

$$Q = -wk_p\bar{h}(cos\theta\frac{\partial\bar{h}}{\partial x} + sin\theta) = -\frac{k_p s}{n}[cos\theta\frac{\partial}{\partial x}(\frac{s}{nw}) + sin\theta] \tag{3}$$

and then substituting Eq. (3) into Eq. (1) results in

$$\frac{\partial s}{\partial t} = \frac{k_p cos\theta}{n^2}\frac{\partial}{\partial x}\left[\frac{s}{w}\left(\frac{\partial s}{\partial x} - \frac{s}{w}\frac{\partial w}{\partial x}\right)\right] + \frac{k_p}{n}sin\theta\frac{\partial s}{\partial x} + Rw \tag{4}$$

where $s \approx n \cdot \bar{h} \cdot w$, n is drainable porosity, k_p is hydraulic conductivity [LT^{-1}], and $\bar{h}$ is average water depth [L]. Note that $\bar{h}$ and R are defined as

$$\bar{h} = \bar{h}(x,t) = \frac{1}{w(x)}\int_w h(x,y,t)\,dy \tag{5}$$

$$R = R(t) = \sum_{k=1}^{n} R_k[U(t - t_{k-1}) - U(t - t_k)] \tag{6}$$

where R_k is the recharge rate within a time step and $U(-)$ is a unit step function.

Because Eq. (4) is a nonlinear equation, solving it analytically is difficult; therefore, the following linearization technique was adopted according to Troch et al. (2003):

$$\frac{s}{w} \simeq b\frac{\bar{s}_c}{\bar{w}} = bnD \tag{7}$$

https://doi.org/10.5194/hess-2021-50
Preprint. Discussion started: 23 February 2021

Hydrology and Earth System Sciences
Discussions

where b is a fitting parameter ($0 \le b \le 1$), $\bar{s_c}$ is average storage capacity [L^2], $\bar{w}$ is the average width of the aquifer [L], and D is the average aquifer depth along the hillslope.

Inserting Eqs. (2) and (7) into Eq. (4) to linearize the nonlinear term yields

$$\frac{\partial s}{\partial t} = \frac{k_p bD\cos\theta}{n}\left(\frac{\partial^2 s}{\partial x^2} - a\frac{\partial s}{\partial x}\right) + \frac{k_p}{n}\sin\theta\frac{\partial s}{\partial x} + Rce^{ax} \quad (8)$$

Equation (8) is a linearized equation and thus can be solved using an analytical approach.

2.2 Initial condition

The distribution of water storage was initially assumed along the x direction as follows:

$$s(x,0) = \gamma n w(x) = \gamma n c e^{ax}, 0 < x < L \quad (9)$$

where γ is the initial constant water depth [L] and $0 \le \gamma \le D$.

2.3 Boundary conditions

According to Brutsaert (1994) and Verhoest and Troch (2000), no influx occurred at the upstream boundary condition (BC; $x = L$), that is,

$$Q = -w\bar{h}k_p\left(\cos\theta\frac{\partial\bar{h}}{\partial x} + \sin\theta\right) = 0, t > 0 \quad (10)$$

which yields

$$\frac{k_p\cos\theta}{n^2}\left[\frac{s}{w}\left(\frac{\partial s}{\partial x} - \frac{s}{w}\frac{\partial w}{\partial x}\right)\right] + \frac{k_p}{n}\sin\theta\cdot s = 0, t > 0 \quad (11)$$

Substituting Eq. (7) into Eq. (11) results in

$$\frac{k_p bD\cos\theta}{n}\frac{\partial s}{\partial x} + \left(\frac{k_p}{n}\sin\theta - \frac{ak_p bD\cos\theta}{n}\right)s = 0, t > 0, x = L \quad (12)$$

Furthermore, the outlet does not store water ($x = 0$) because water is drained out by a channel:

$$s(0,t) = 0, t > 0 \quad (13)$$

2.4 Analytical solution

To solve Eq. (8) associated with Eqs. (9), (12), and (13), the integral transforms presented by Özisik (1968) were introduced as follows:

Integral transform:

$$\bar{P}(\beta_m, t) = \int_{x'=0}^{L} K(\beta_m, x')\, P(x', t)dx' \quad (14)$$

Inverse transform:

$$P(x,t) = \sum_{m=1}^{\infty} K(\beta_m, x)\,\bar{P}(\beta_m, t) \quad (15)$$

where $K(\beta_m, x)$ is the kernel function and $\bar{P}$ is the transformed function of P.

Before the aforementioned problem was solved, Eq. (8) was rewritten as

https://doi.org/10.5194/hess-2021-50
Preprint. Discussion started: 23 February 2021

$$\frac{\partial s}{\partial t} = A\frac{\partial^2 s}{\partial x^2} + B\frac{\partial s}{\partial x} + Rce^{ax} \tag{16}$$

where $A = \frac{k_p bD}{n} cos\theta$, $B = \frac{k_p}{n} sin\theta - \frac{ak_p bD}{n} cos\theta$.

Next, Eq. 17 is set as follows:

$$s(x,t) = e^{-\frac{B}{2A}x} e^{-\frac{B^2}{4A}t} s^*(x,t) \tag{17}$$

and substituting Eq. (17) into Eqs. (16), (9), (12), and (13) results in

$$\frac{1}{A}\frac{\partial s^*}{\partial t} = \frac{\partial^2 s^*}{\partial x^2} + g(x,t) \tag{18}$$

$$s^*(x,0) = \gamma nce^{\left(a+\frac{B}{2A}\right)x}, 0 < x < L \tag{19}$$

$$A\frac{\partial s^*}{\partial x} + \frac{B}{2}s^* = 0, t > 0, x = L \tag{20}$$

$$\mathrm{s}^*(0,\mathrm{t}) = 0, \mathrm{t} > 0 \tag{21}$$

where $g(x,t) = \frac{R(t)c}{A} e^{(a+\frac{B}{2A})x} e^{\frac{B^2}{4A}t}$.

Taking the integral transform of Eqs. (18)–(21) yields

$$\frac{d\bar{s}^*(\beta_m,t)}{dt} + A \cdot {\beta_m}^2 \cdot \bar{s}^*(\beta_m,t) = A \cdot \bar{g}(\beta_m,t) \tag{22}$$

$$\bar{s}^*(\beta_m,0) = \int_{x'=0}^{L} K(\beta_m,x')\,\gamma nce^{\left(a+\frac{B}{2A}\right)x'} dx' \equiv \bar{F}(\beta_m) \tag{23}$$

with the kernel

$$K(\beta_m,x) = \left[\frac{2\left({\beta_m}^2+{B^2}/{4A^2}\right)}{L\left({\beta_m}^2+{B^2}/{4A^2}\right)+{B}/{2A}}\right]^{1/2} \cdot sin(\beta_m x) \tag{24}$$

and

$$\bar{g}(\beta_m,t) = \int_{x'=0}^{L} K(\beta_m,x')\,\frac{R(t)c}{A} e^{(a+\frac{B}{2A})x'} e^{\frac{B^2}{4A}t}\, dx' \tag{25}$$

where β_m ($m \in \boldsymbol{N}$, a natural number) is the root of the following eigen equation:

$$\beta cot(\beta L) = -\frac{B}{2A} \tag{26}$$

Notably, the eigenvalue β_m is affected by the slope θ, the fitting parameter b, the average aquifer depth D, and the parameter a.

Solving Eq. (22) associated with Eqs. (23)–(26) yields

https://doi.org/10.5194/hess-2021-50
Preprint. Discussion started: 23 February 2021

$$\bar{s}^*(\beta_m,t) = e^{-A\beta_m{}^2 t}\left[\bar{F}(\beta_m) + \int_{t'=0}^{t} e^{A\beta_m{}^2 t'} A\bar{g}(\beta_m,t')dt'\right] \tag{27}$$

Taking inverse transform of $\bar{s}$ results in

$$s^*(x,t) = \sum_{m=1}^{\infty} e^{-A\beta_m{}^2 t}\left[\bar{F}(\beta_m) + \int_{t'=0}^{t} e^{A\beta_m{}^2 t'} A\bar{g}(\beta_m,t')dt'\right] \tag{28}$$

By employing Eq. (17), we can obtain

$$s(x,t) = 2ce^{\frac{-B}{2A}x}e^{\frac{-B^2}{4A}t}\sum_{m=1}^{\infty}\frac{\beta_m-\beta_m e^{\left(a+\frac{B}{2A}\right)L}\cos(\beta_m L)+\left(a+\frac{B}{2A}\right)e^{\left(a+\frac{B}{2A}\right)L}sin(\beta_m L)}{\left(a+\frac{B}{2A}\right)^2+\beta_m{}^2}\cdot$$

$$\frac{\beta_m{}^2+B^2/_{4A^2}}{L\left(\beta_m{}^2+B^2/_{4A^2}\right)+B/_{2A}}[\gamma n+R(t)\frac{e^{\left(A\beta_m{}^2+\frac{B^2}{4A}\right)t}-1}{A\beta_m{}^2+\frac{B^2}{4A}}]e^{-A\beta_m{}^2 t}sin(\beta_m x) \tag{29}$$

After the storage was obtained, the water level (h), discharge (Q), outflow rate (q), and relative storage (s_r) were calculated, respectively, as follows:

$$\bar{h}(x,t) = \frac{s}{n\cdot w(x)} = \frac{2}{n\cdot e^{ax}}\,e^{\frac{-B}{2A}x}e^{\frac{-B^2}{4A}t}\sum_{m=1}^{\infty}\frac{\beta_m-\beta_m e^{\left(a+\frac{B}{2A}\right)L}cos(\beta_m L)+(a+\frac{B}{2A})e^{\left(a+\frac{B}{2A}\right)L}sin(\beta_m L)}{\left(a+\frac{B}{2A}\right)^2+\beta_m{}^2}\cdot$$

$$\left[\frac{\beta_m{}^2+B^2/_{4A^2}}{L\left(\beta_m{}^2+B^2/_{4A^2}\right)+B/_{2A}}\right]\left[\gamma n+R(t)\frac{e^{\left(A\beta_m{}^2+\frac{B^2}{4A}\right)t}-1}{A\beta_m{}^2+\frac{B^2}{4A}}\right]e^{-A\beta_m{}^2 t}\sin(\beta_m x) \tag{30}$$

$$Q(x,t) = (2B-Bcos\theta)ce^{\frac{-B}{2A}x}e^{\frac{-B^2}{4A}t}\sum_{m=1}^{\infty}\frac{\beta_m-\beta_m e^{\left(a+\frac{B}{2A}\right)L}\cos(\beta_m L)+\left(a+\frac{B}{2A}\right)e^{\left(a+\frac{B}{2A}\right)L}sin(\beta_m L)}{\left(a+\frac{B}{2A}\right)^2+\beta_m{}^2}\cdot$$

$$\frac{\beta_m{}^2+B^2/_{4A^2}}{L\left(\beta_m{}^2+B^2/_{4A^2}\right)+B/_{2A}}[e^{-A\beta_m{}^2 t}\gamma n+R(t)\frac{e^{\left(A\beta_m{}^2+\frac{B^2}{4A}\right)t}-1}{A\beta_m{}^2+\frac{B^2}{4A}}]\sin(\beta_m x)+$$

$$2Acos\theta e^{\frac{-B}{2A}x}e^{\frac{-B^2}{4A}t}\sum_{m=1}^{\infty}\frac{\beta_m-\beta_m e^{\left(a+\frac{B}{2A}\right)L}cos(\beta_m L)+\left(a+\frac{B}{2A}\right)e^{\left(a+\frac{B}{2A}\right)L}\sin(\beta_m L)}{\left(a+\frac{B}{2A}\right)^2+\beta_m{}^2}$$

$$\frac{\beta_m(\beta_m{}^2+B^2/_{4A^2})}{L\left(\beta_m{}^2+B^2/_{4A^2}\right)+B/_{2A}}\left[e^{-A\beta_m{}^2 t}\gamma n+R(t)\frac{e^{\left(A\beta_m{}^2+\frac{B^2}{4A}\right)t}-1}{A\beta_m{}^2+\frac{B^2}{4A}}\right]cos(\beta_m x) \tag{31}$$

$$q(t) = 2Acos\theta e^{\frac{-B^2}{4A}t}\sum_{m=1}^{\infty}\frac{\beta_m-\beta_m e^{\left(a+\frac{B}{2A}\right)L}cos(\beta_m L)+(a+\frac{B}{2A})e^{\left(a+\frac{B}{2A}\right)L}sin(\beta_m L)}{\left(a+\frac{B}{2A}\right)^2+\beta_m{}^2}$$

$$\frac{\beta_m(\beta_m{}^2+B^2/_{4A^2})}{L\left(\beta_m{}^2+B^2/_{4A^2}\right)+B/_{2A}}[e^{-A\beta_m{}^2 t}\gamma n+R(t)\frac{e^{\left(A\beta_m{}^2+\frac{B^2}{4A}\right)t}-1}{A\beta_m{}^2+\frac{B^2}{4A}}] \tag{32}$$

https://doi.org/10.5194/hess-2021-50
Preprint. Discussion started: 23 February 2021

Hydrology and Earth System Sciences
Discussions
Open Access

$$s_r(x,t) = \frac{s}{n \cdot D \cdot w(x)} = \frac{2}{n \cdot D \cdot e^{ax}} e^{\frac{-B}{2A}x} e^{\frac{-B^2}{4A}t}$$

$$\sum_{m=1}^{\infty} \frac{\beta_m - \beta_m e^{\left(a+\frac{B}{2A}\right)L} cos(\beta_m L) + (a+\frac{B}{2A}) e^{\left(a+\frac{B}{2A}\right)L} sin(\beta_m L)}{\left(a+\frac{B}{2A}\right)^2 + {\beta_m}^2} \left[\frac{{\beta_m}^2 + B^2/_{4A^2}}{L\left({\beta_m}^2 + B^2/_{4A^2}\right) + B/_{2A}}\right] [\gamma n +$$

$$R(t) \frac{e^{\left(A{\beta_m}^2 + \frac{B^2}{4A}\right)t} - 1}{A{\beta_m}^2 + \frac{B^2}{4A}}] e^{-A{\beta_m}^2 t} sin(\beta_m x) \qquad (33)$$

The generalized integral transform technique was employed to acquire the above analytical solutions because its convergence of the solution is better than that by the Laplace transform method (Wu and Hsieh, 2019).

2.5 Numerical method

In addition to using an analytical approach to solve the linearized equation, Eq. (8), a numerical model was developed to solve the original nonlinear equation, Eq. (4). With reference to Swanson and Turke (1990), the upwind scheme and central difference of finite difference method were used to discretize the space, and with reference to Shu and Osher (1989), the third-order TVD Runge–Kutta scheme was applied to deal with time. The space was divided into *m* + 1 nodes with an equal interval of Δx along the *x* direction, in which the nodes $i = 1$ and $i = m+1$ are virtual outside the domain (Fig. 2). The difference equation for space discretization of water storage is as follows:

$$\frac{\partial {s_\alpha}^j}{\partial t} = \frac{k_p cos\theta}{n^2} \left[\frac{\frac{{s_\alpha}^j(i+1)}{w(i+1)} + \frac{{s_\alpha}^j(i)}{w(i)}}{2\Delta x} \frac{{s_\alpha}^j(i+1) - {s_\alpha}^j(i)}{\Delta x} - \frac{\frac{{s_\alpha}^j(i)}{w(i)} + \frac{{s_\alpha}^j(i-1)}{w(i-1)}}{2\Delta x} \frac{{s_\alpha}^j(i) - {s_\alpha}^j(i-1)}{\Delta x} - \right.$$

$$\left. \frac{\left(\frac{\frac{{s_\alpha}^j(i+1)}{w(i+1)} + \frac{{s_\alpha}^j(i)}{w(i)}}{2}\right)^2}{\Delta x} \frac{w(i+1) - w(i)}{\Delta x} + \frac{\left(\frac{\frac{{s_\alpha}^j(i)}{w(i)} + \frac{{s_\alpha}^j(i-1)}{w(i-1)}}{2}\right)^2}{\Delta x} \frac{w(i) - w(i-1)}{\Delta x}\right] + \frac{k_p}{n} sin\theta \frac{{s_\alpha}^j(i+1) - {s_\alpha}^j(i)}{\Delta x} + R^j w(i) \qquad (34)$$

where *i* is the node number (*i* = 1,2,…,*m* + 1), *j* is time, and s_α is the solution of order α. Furthermore, from Eq. (9), the initial condition becomes

$${s_\alpha}^j(i) = \gamma n c e^{a x_i}, \ i = 1,2,\dots,m+1, j = 0 \qquad (35)$$

and the BC becomes

1. No flux at the upstream BC

$$\frac{1}{\Delta x}\left[\frac{{s_\alpha}^j(m+1)}{w(m+1)} - \frac{{s_\alpha}^j(m)}{w(m)}\right] + ntan\theta = 0$$

$$\Rightarrow {s_\alpha}^j(m+1) = \frac{{s_\alpha}^j(m)}{w(m)} - ntan\theta \cdot w(m+1) \cdot \Delta x, j > 0 \qquad (36)$$

2. No storage at the downstream BC (Taylor series expansion to increase accuracy)

$$s_\alpha{}^j(1) = -2s_\alpha{}^j(2) + \frac{1}{3}s_\alpha{}^j(3) \tag{37}$$

Regarding the discretization in time, the third-order TVD Runge–Kutta method yields the following:

$$s_1 = s_0 + \Delta t\Phi(s_0) \tag{38}$$

$$s_2 = s_1 + \frac{\Delta t}{4}[-3\Phi(s_0) + \Phi(s_1)] \tag{39}$$

$$s_3 = s_2 + \frac{\Delta t}{12}[-\Phi(s_0) - \Phi(s_1) + 8\Phi(s_2)] \tag{40}$$

where s_1, s_2, and s_3 are the solutions of each order. $\Phi(s) = \frac{\partial s}{\partial t}$. s_0 is the initial condition. The final difference equation is listed in Appendix A.

3 Results and Discussion

3.1 Verification of the analytical solution

To validate the present analytical solution, the following parameter values presented by Troch et al. (2004) were adopted: slope length L = 100 m, slope θ = 5%, n = 0.3, b = 1, D = 2 m, k_p = 1 mh^{-1}, initial water depth γ = 0.4 m, and R = 10 mmd^{-1}. The values of the parameters in Eq. (2) controlling the width and shape were $a = 0.02\ \mathrm{m}^{-1}$ and $c = 6.77$ m for a convergent hillslope, $a = 0$ and $c = 21.627$ m for a uniform hillslope, and $a = -0.02\ \mathrm{m}^{-1}$ and $c = 50.024$ m for a divergent hillslope. The projected areas of all three hillslopes were the same size (2162.7 m^2), so they received the same rainfall recharge. The received volume was 4325.4 m^3, and the initial water storage was also assumed to be consistent.

Figure 3 illustrates the spatial variation of groundwater levels for different shapes for 1, 5, and 20 days, and Fig. 4 presents the temporal variation of flow rates at the outlet for different shapes. Both figures reveal that our results using the generalized integral transform technique agree well with the Laplace transform method by Troch et al. (2004), thus validating our analytical solutions. However, we could not use the Laplace transform method directly in the present study for two reasons. First, the inverse Laplace transform is too complex, and finding the function is challenging even after performing the inverse Laplace transform. Second, the convergence of solutions using our approach was better than that obtained by the Laplace transform method as discussed in Wu and Hsieh (2019). Compared with Verhoest and Troch (2000), whose solution summation requires the first 999 terms, namely O(10^3), to reach convergence, the present solution requires only the first O(10^2) terms, leading to a convergence that is more than 10 times faster.

https://doi.org/10.5194/hess-2021-50
Preprint. Discussion started: 23 February 2021

3.2 Verification of the numerical solution

With reference to Troch et al. (2003), two cases are illustrated. Case 1 had no rainfall recharge but did have initial water depth, and Case 2 had no initial water depth but did have rainfall recharge. The simulated representative hillslope type was uniform ($a = 0$ and $c = 50$ m), and the following parameters were adopted: L = 100 m, $\theta = 5\%$, n = 0.3, D = 2 m, k_p= 1 mh^{-1}, γ = 0 and 0.4 m, and R = 0 and 10 mmd^{-1}.

Figures 5 and 6 present the variation in relative storage for Case 1 with γ = 0.4 m and Case 2 with R = 10 mmd^{-1}, respectively. Again, the results agree well with those of Troch et al. (2003), thus validating the present numerical solution.

3.3 Comparison between analytical solutions and numerical solutions

With the parameters D = 2 m and γ = 1 m, the simulated results for convergent hillslope are shown in Figs. 7–9, in which parameter b was selected for better simulated results. When (R, b) = (50, 0.5–0.7), (25, 0.3), and (10, 0.2) in Figs. 7–9, respectively, an obvious discrepancy was noted between the analytical and numerical solutions for different durations. The averaged absolute relative percentage differences were 2.78% when b = 0.2 and 3.93% when b = 0.7 in Fig. 7(a), 16.09% when b = 0.5 and 8.72% when b = 0.7 in Fig. 7(b), and 35.49% when b = 0.5 and 23.76% when b = 0.7 in Fig. 7(c). These results indicate that the discrepancy increased with duration even when an optimal fitting parameter b was selected. Similar trends can be observed in Figs. 8 and 9. Furthermore, the shift became relatively large for a higher recharge rate (R = 50 mmd^{-1} in Fig. 7) and smaller for a lower recharge rate (R = 10 mmd^{-1} in Fig. 9) especially for a longer period. Similar trends were found for a uniform hillslope when (R, b) = (50, 0.3), (25, 0.2), and (10, 0.2) in Figs. 10–12, respectively, and for divergent hillslope when (R, b) = (50, 0.2), (25, 0.1), and (10, 0.08) in Figs. 13–15, respectively.

Taken together, the aforementioned results imply that the present analytical solutions are highly sensitive to the fitting parameter b. In fact, the parameter b in Eq. (7) is affected by hill storage, aquifer width, and aquifer thickness. Therefore, adjusting b for different hillslope types and different recharge rates can bring the analytical results closer to the numerical results. In this study, the fitting parameter b was determined using trial and error. To summarize, the optimal parameter b is relatively large for convergent hillslope but relatively small for divergent hillslope. The parameter b also increases with the recharge rate. As the recharge rate increases, the water storage increases, and the discrepancy between both solutions also increases, especially for convergent hillslopes.

https://doi.org/10.5194/hess-2021-50
Preprint. Discussion started: 23 February 2021

3.4 Variation of the remaining hill storage

To obtain the remaining hill storage at any time for the three hillslopes with any constant slope, the parameter s', which denotes the dimensionless remaining amount of hill-storage water, was defined as follows:

$$s'(t) = \frac{\int_0^L s(x,t)dx}{\int_0^L s(x,0)dx} \approx \frac{\sum_0^{x=L} s(x,t)\Delta x}{\sum_0^{x=L} s(x,0)\Delta x} \tag{41}$$

Because the numerical solutions were obtained by solving the nonlinear Boussinesq equation, which is more complete, the discussion hereafter is based on the numerical model. When a 1-day duration was used as an example with θ = 5% and no recharge, the remaining convergent:uniform:divergent storage ratio was approximately 1:0.984:0.888; when θ = 15%, the ratio became 1:0.937:0.785; θ = 30%, 1:0.826:0.572; θ = 40%, 1:0.826:0.572; θ = 55%, 1:0.779:0.488; θ = 100%, 1:0.688:0.359. As expected, water drained the fastest on the steepest divergent hillslopes. Figures 16–18 demonstrate that when the slope and simulation duration increased, the remaining hill storage decreased. To summarize, the reduction rate of hill storage became large for steep slopes, especially for divergent hillslopes.

3.5 Temporally varied recharge rates effect

Because the recharge rate is not uniformly distributed, this study considered it to have temporal variation. Assuming $\theta = 5\%$, D = 5 m, and γ = 0, three patterns of recharge distribution variation (Fig. 19) were considered to discuss their effects on hill storage. Figure 20 illustrates the spatial variation of the water table under different recharge types for a convergent hillslope at different durations. The simulated scenarios had the same aquifer and groundwater conditions, except for the recharge patterns. The results reveal that the water table was significantly affected by the recharge type within a short period (12 h), but after 1 day, it was almost no longer affected by the recharge type. Similar results were obtained for uniform and divergent hillslopes.

We added three more recharge types: peak in the first section, peak in the last section, and double peak; Fig. 21 illustrates the variation of outflow for different hillslopes under six types of recharge. Figure 21(a) demonstrates that each outflow peak was different and that the maximum peak occurred at the curve of peak in the last section, but all outflows gradually approached one value for the convergent hillslope under the same accumulative recharge amount. Similar results are found in Fig. 21(b) and 21(c) for uniform and divergent hillslopes, respectively. Furthermore, the cross-sectional area at the outlet for the convergent hillslope was relatively small; thus, the flow rate was the lowest. By contrast, the cross-sectional area at the

https://doi.org/10.5194/hess-2021-50
Preprint. Discussion started: 23 February 2021

Hydrology and Earth System Sciences
Open Access
Discussions

outlet for the divergent hillslope was relatively large; thus, the flow rate was the highest. These hydraulic characteristics are indicated in Fig. 21(a) and 21(c). Figure 21 also illustrates that when the recharge ceases, the outflow for convergent hillslopes decreases and then gently increases for a long period due to the slow release of hill-stored water. For uniform hillslopes, the outflow reduces slowly when the recharge stops, but for divergent hillslopes, the outflow drops more rapidly owing to the fast water release.

4 Concluding remarks

To elucidate water storage of different hillslopes with variable width under any type of temporally varied rainfall recharge, both analytical and numerical approaches were employed to solve the Boussinesq equation. Numerical solutions to the nonlinear hillslope-storage equation and analytical solutions to the linearized hillslope-storage equation were subsequently presented. A summary of our findings is as follows:

1. The analytical solutions were derived using the generalized integral transform technique and verified with the method of Troch et al. (2004), which was derived using the Laplace transform method. The results were consistent for convergent, uniform, and divergent hillslopes. Our numerical solutions agreed well with the results of Troch et al. (2003), which were obtained through the numerical integration of the partial differential equation.
2. Although our analytical solutions were verified with previous analytical solutions, the results need tuning of the parameter b to better fit the results of the numerical model in the same scenarios. The results reveal that as the recharge increases, b increases, with b being the largest for convergent hillslopes and the smallest for divergent hillslopes.
3. Comparison of the analytical and numerical results reveals that especially for convergent hillslopes, when the recharge decreases, the discrepancy between the results also decreases.
4. For the same hillslope, the hillslope storage of water decreases as the slope increases because water drains fast along a steep slope. For the same slope and recharge distribution, water storage is the most abundant for convergent hillslopes because of slow drainage and least for divergent hillslopes because of rapid drainage.

The findings of the present study thus can be useful for father research and have value in the practical application of the soil and water conservation issue.

https://doi.org/10.5194/hess-2021-50
Preprint. Discussion started: 23 February 2021

Appendix A

Difference equations of the hill-storage equation

$$s_1{}^j(i) = s_0{}^j + \Delta t \cdot \{\frac{k_p cos\theta}{n^2}[\frac{\frac{s_0{}^j(i+1)}{w(i+1)}+\frac{s_0{}^j(i)}{w(i)}}{2\Delta x}\frac{s_0{}^j(i+1)-s_0{}^j(i)}{\Delta x} - \frac{\frac{s_0{}^j(i)}{w(i)}+\frac{s_0{}^j(i-1)}{w(i-1)}}{2\Delta x}\frac{s_0{}^j(i)-s_0{}^j(i-1)}{\Delta x} - \frac{(\frac{\frac{s_0{}^j(i+1)}{w(i+1)}+\frac{s_0{}^j(i)}{w(i)}}{2})^2}{\Delta x}\frac{w(i+1)-w(i)}{\Delta x} + \frac{(\frac{\frac{s_0{}^j(i)}{w(i)}+\frac{s_0{}^j(i-1)}{w(i-1)}}{2})^2}{\Delta x}\frac{w(i)-w(i-1)}{\Delta x}] + \frac{k_p}{n} sin\theta \frac{s_0{}^j(i+1)-s_0{}^j(i)}{\Delta x} + R^j w(i)\} \quad (A.1)$$

$$s_2{}^j(i) = s_1{}^j + \frac{-3\Delta t}{4} \cdot \{\frac{k_p cos\theta}{n^2}[\frac{\frac{s_0{}^j(i+1)}{w(i+1)}+\frac{s_0{}^j(i)}{w(i)}}{2\Delta x}\frac{s_0{}^j(i+1)-s_0{}^j(i)}{\Delta x} - \frac{\frac{s_0{}^j(i)}{w(i)}+\frac{s_0{}^j(i-1)}{w(i-1)}}{2\Delta x}\frac{s_0{}^j(i)-s_0{}^j(i-1)}{\Delta x} - \frac{(\frac{\frac{s_0{}^j(i+1)}{w(i+1)}+\frac{s_0{}^j(i)}{w(i)}}{2})^2}{\Delta x}\frac{w(i+1)-w(i)}{\Delta x} + \frac{(\frac{\frac{s_0{}^j(i)}{w(i)}+\frac{s_0{}^j(i-1)}{w(i-1)}}{2})^2}{\Delta x}\frac{w(i)-w(i-1)}{\Delta x}] + \frac{k_p}{n} sin\theta \frac{s_0{}^j(i+1)-s_0{}^j(i)}{\Delta x} + R^j w(i)\} + \frac{\Delta t}{4} \cdot \{\frac{k_p cos\theta}{n^2}[\frac{\frac{s_1{}^j(i+1)}{w(i+1)}+\frac{s_1{}^j(i)}{w(i)}}{2\Delta x}\frac{s_1{}^j(i+1)-s_1{}^j(i)}{\Delta x} - \frac{\frac{s_1{}^j(i)}{w(i)}+\frac{s_1{}^j(i-1)}{w(i-1)}}{2\Delta x}\frac{s_1{}^j(i)-s_1{}^j(i-1)}{\Delta x} - \frac{(\frac{\frac{s_1{}^j(i+1)}{w(i+1)}+\frac{s_1{}^j(i)}{w(i)}}{2})^2}{\Delta x}\frac{w(i+1)-w(i)}{\Delta x} + \frac{(\frac{\frac{s_1{}^j(i)}{w(i)}+\frac{s_1{}^j(i-1)}{w(i-1)}}{2})^2}{\Delta x}\frac{w(i)-w(i-1)}{\Delta x}] + \frac{k_p}{n} sin\theta \frac{s_1{}^j(i+1)-s_1{}^j(i)}{\Delta x} + R^j w(i)\} \quad (A.2)$$

$$s_3{}^j(i) = s_2{}^j + \frac{-\Delta t}{12} \cdot \{\frac{k_p cos\theta}{n^2}[\frac{\frac{s_0{}^j(i+1)}{w(i+1)}+\frac{s_0{}^j(i)}{w(i)}}{2\Delta x}\frac{s_0{}^j(i+1)-s_0{}^j(i)}{\Delta x} - \frac{\frac{s_0{}^j(i)}{w(i)}+\frac{s_0{}^j(i-1)}{w(i-1)}}{2\Delta x}\frac{s_0{}^j(i)-s_0{}^j(i-1)}{\Delta x} - \frac{(\frac{\frac{s_0{}^j(i+1)}{w(i+1)}+\frac{s_0{}^j(i)}{w(i)}}{2})^2}{\Delta x}\frac{w(i+1)-w(i)}{\Delta x} + \frac{(\frac{\frac{s_0{}^j(i)}{w(i)}+\frac{s_0{}^j(i-1)}{w(i-1)}}{2})^2}{\Delta x}\frac{w(i)-w(i-1)}{\Delta x}] + \frac{k_p}{n} sin\theta \frac{s_0{}^j(i+1)-s_0{}^j(i)}{\Delta x} + R^j w(i)\} - \frac{\Delta t}{12} \cdot \{\frac{k_p cos\theta}{n^2}[\frac{\frac{s_1{}^j(i+1)}{w(i+1)}+\frac{s_1{}^j(i)}{w(i)}}{2\Delta x}\frac{s_1{}^j(i+1)-s_1{}^j(i)}{\Delta x} - \frac{\frac{s_1{}^j(i)}{w(i)}+\frac{s_1{}^j(i-1)}{w(i-1)}}{2\Delta x}\frac{s_1{}^j(i)-s_1{}^j(i-1)}{\Delta x} - \frac{(\frac{\frac{s_1{}^j(i+1)}{w(i+1)}+\frac{s_1{}^j(i)}{w(i)}}{2})^2}{\Delta x}\frac{w(i+1)-w(i)}{\Delta x} + \frac{(\frac{\frac{s_1{}^j(i)}{w(i)}+\frac{s_1{}^j(i-1)}{w(i-1)}}{2})^2}{\Delta x}\frac{w(i)-w(i-1)}{\Delta x}] + \frac{k}{n} sin\theta \frac{s_1{}^j(i+1)-s_1{}^j(i)}{\Delta x} + R^j w(i)\} + \frac{2\Delta t}{3} \cdot \{\frac{k_p cos\theta}{n^2}[\frac{\frac{s_2{}^j(i+1)}{w(i+1)}+\frac{s_2{}^j(i)}{w(i)}}{2\Delta x}\frac{s_2{}^j(i+1)-s_2{}^j(i)}{\Delta x} - \frac{\frac{s_2{}^j(i)}{w(i)}+\frac{s_2{}^j(i-1)}{w(i-1)}}{2\Delta x}\frac{s_2{}^j(i)-s_2{}^j(i-1)}{\Delta x} - \frac{(\frac{\frac{s_2{}^j(i+1)}{w(i+1)}+\frac{s_2{}^j(i)}{w(i)}}{2})^2}{\Delta x}\frac{w(i+1)-w(i)}{\Delta x} + \frac{(\frac{\frac{s_2{}^j(i)}{w(i)}+\frac{s_2{}^j(i-1)}{w(i-1)}}{2})^2}{\Delta x}\frac{w(i)-w(i-1)}{\Delta x}] + \frac{k_p}{n} sin\theta \frac{s_2{}^j(i+1)-s_2{}^j(i)}{\Delta x} + R^j w(i) \quad (A.3)$$

Author contribution: Conceptualization: P.C. Hsieh; Formal analysis: T.T. Huang and P.C. Hsieh; Funding acquisition: P.C. Hsieh; Investigation: T.T. Huang and P.C. Hsieh;

Methodology: T.T. Huang and P.C. Hsieh; Resources: P.C. Hsieh; Software: T.T. Huang; Supervision: P.C. Hsieh; Validation: T.T. Huang; Visualization: P.C. Hsieh; Writing – original draft preparation: P.C. Hsieh; Writing – review & editing: P.C. Hsieh.

Competing interests: The authors declare that they have no conflict of interest.

Acknowledgements

This study was financially supported by the Ministry of Science and Technology of Taiwan under Grant No.: MOST 109-2313-B-005-037.

References

Anderson, M. G. and Burt, T. P.: The role of topography in controlling throughflow generation, Earth Surf. Proc., 3, 331-344, 1978.

Brutsaert, W.: The unit response of groundwater outflow from a hillslope, Water Resour. Res., 30, 2759-2763, 1994.

Childs, E.: Drainage of groundwater resting on a sloping bed, Water Resour. Res., 7, 1256-1263, 1971.

Evans I. S.: An integrated system of terrain analysis and slope mapping, Department of Geography, University of Durham, 1979.

Fan, Y. and Bras, R.: Analytical solutions to hillslope subsurface storm flow and saturation overland flow. Water Resour. Res. 34, 921-927, 1998.

https://doi.org/10.5194/hess-2021-50
Preprint. Discussion started: 23 February 2021

Hydrology and Earth System Sciences
Discussions

Genereux, D. P., Hemond, H. F., and Mulholland, P. J.: Spatial and temporal variability in streamflow generation on the West Fork of Walker Branch Watershed, J. Hydrol., 142, 137-166, 1993.

Kazezyilmaz-Alhan, C. M.: An improved solution for diffusion waves to overland flow, Applied Math. Model., 36, 1465-4172, 2012.

Li, H., Jiao, J. J., Luk, M., and Cheung, K.: Tide-induced groundwater level fluctuation in coastal aquifers bounded by L-shaped coastlines, Water Resour. Res., 38(3), 6.1-6.8, 2002.

McDonnell, J. J.: A rationale for old water discharge through macropores in a steep, humid catchment. Water Resour. Res., 26(11), 2821-2832, 1990.

Mosley, M. P.: Streamflow generation in a forested watershed, New Zealand. Water Resour. Res., 15, 795-806, 1979.

O'Loughlin, E. M.: Prediction of surface saturation zones in natural catchments by topographic analysis, Water Resour. Res., 22, 794-804, 1986.

Özisik, M. N.: Boundary value problems of heat conduction, Dover Publications, INC., New York, 1968.

Shu, C. W.: Total-variation-diminishing time discretizations, SIAM J. Sci. Stat. Comp., 9, 1073–1084, 1988.

Swanson, R. C. and Turkel E.: On central-difference and upwind schemes, J. Comp. Phys., 101(2). 292-306, 1992.

Troch, P. A., van Loon, E. E., and Hilberts, A.: Analytical solutions to a hillslope-storage kinematic wave equation for subsurface flow, Adv. Water Resour., 25, 637-649, 2002.

Troch, P. A., Paniconi, C., and van Loon, E. E.: The hillslope-storage Boussinesq model for subsurface flow and variable source areas along complex hillslopes: 1. Formulation and characteristic response, Water Resour. Res., 39(11), 1316, doi:10.1029/2002WR001728, 2003.

Troch, P. A., van Loon, A. H., and Hilberts, Arno G. J.: Analytical solution of the linearized hillslope-storage Boussinesq equation for exponential hillslope width functions, Water Resour. Res. 40, W08601, doi:10.1029/2003WR002850, 2004.

Verhoest, N. E. C., and Troch, P. A.: Some analytical solutions of the linearized Boussinesq equation with recharge for a sloping aquifer, Water Resour. Res., 36(3), 793-800, 2000.

Woods, R., and Rowe, L.: The changing spatial variability of subsurface flow across a hillside, J. Hydrol., 35, 51-86, 1996.

Woods, R., Sivapalan, M., and Robinson, J.: Modeling the spatial variability of subsurface runoff using a topographic index, Water Resour. Res., 33, 1061-1073, 1997.

Wu, M. C. and Hsieh, P. C.: Improved solutions to the linearized Boussinesq equation with temporally varied rainfall recharge for a sloping aquifer, Water 11, 826;

https://doi.org/10.5194/hess-2021-50
Preprint. Discussion started: 23 February 2021

DOI:10.3390/w11040826, 2019.

https://doi.org/10.5194/hess-2021-50
Preprint. Discussion started: 23 February 2021

Hydrology and Earth System Sciences
Discussions

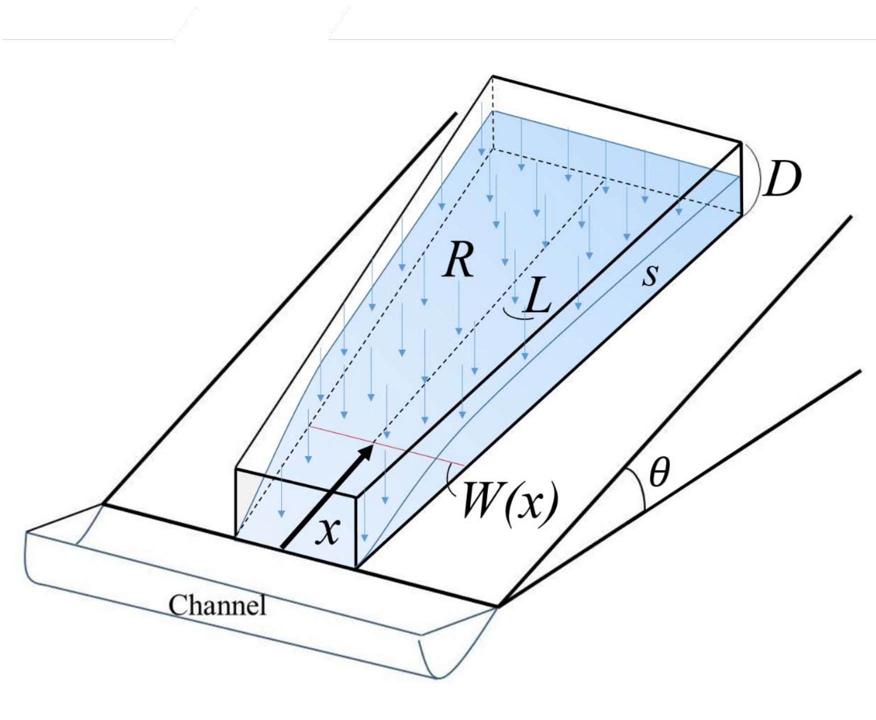

Fig. 1. Schematic of this study.

https://doi.org/10.5194/hess-2021-50
Preprint. Discussion started: 23 February 2021

Hydrology and Earth System Sciences
Discussions

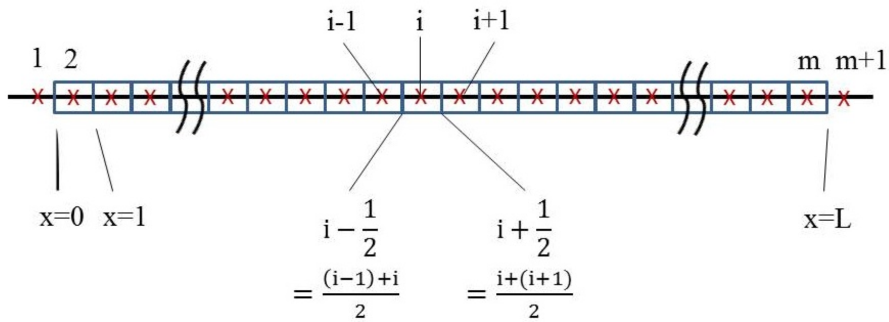

Fig. 2. Schematic of mesh for numerical method.

https://doi.org/10.5194/hess-2021-50
Preprint. Discussion started: 23 February 2021

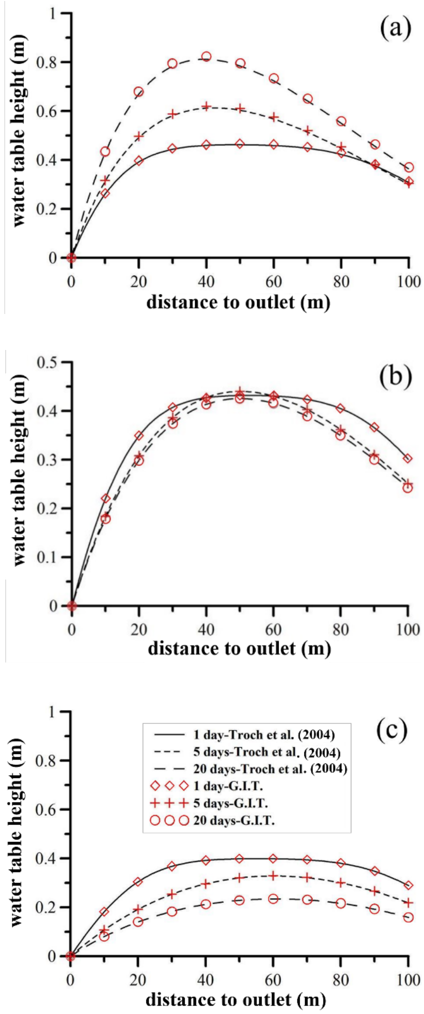

Fig. 3. Verification of the present solutions of groundwater levels for (a) convergent (b) uniform, and (c) divergent hillslopes.

https://doi.org/10.5194/hess-2021-50
Preprint. Discussion started: 23 February 2021

Hydrology and Earth System Sciences
Discussions

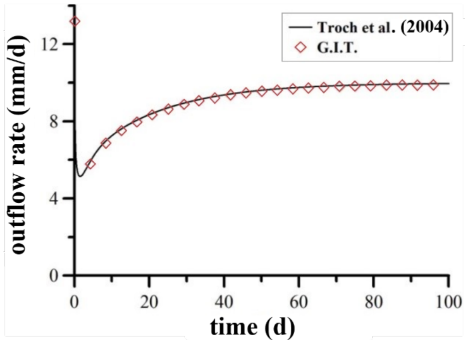

(a) convergent hillslope

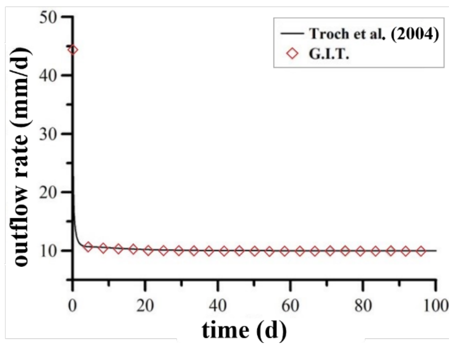

(b) uniform hillslope

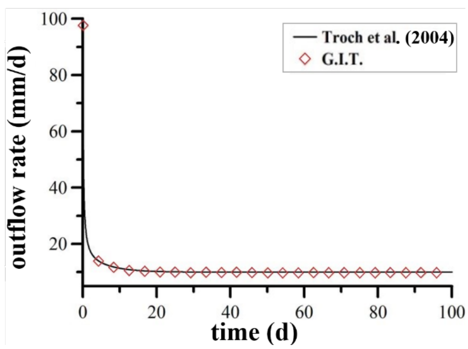

(c) divergent hillslope

Fig. 4. Verification of the present solutions of outflow hydrograph for three hillslope types.

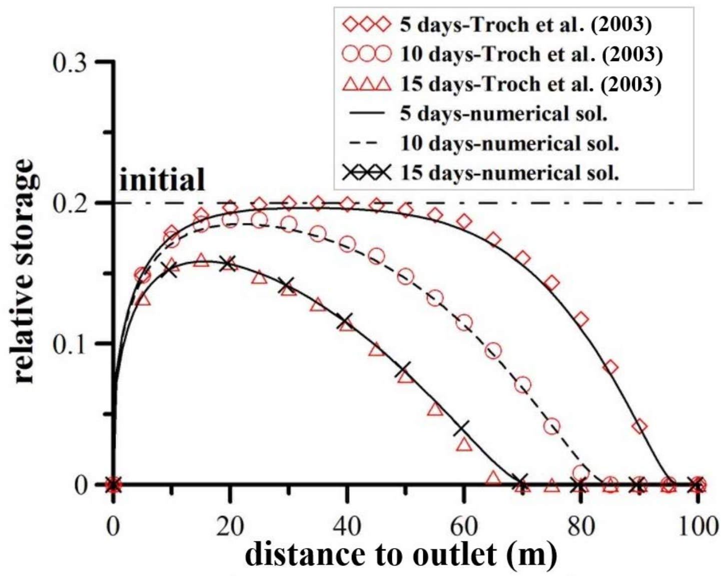

Fig. 5. Comparison of spatial variation of relative storage between the present solutions and previous numerical solutions for γ = 0.4m, and R = 0.

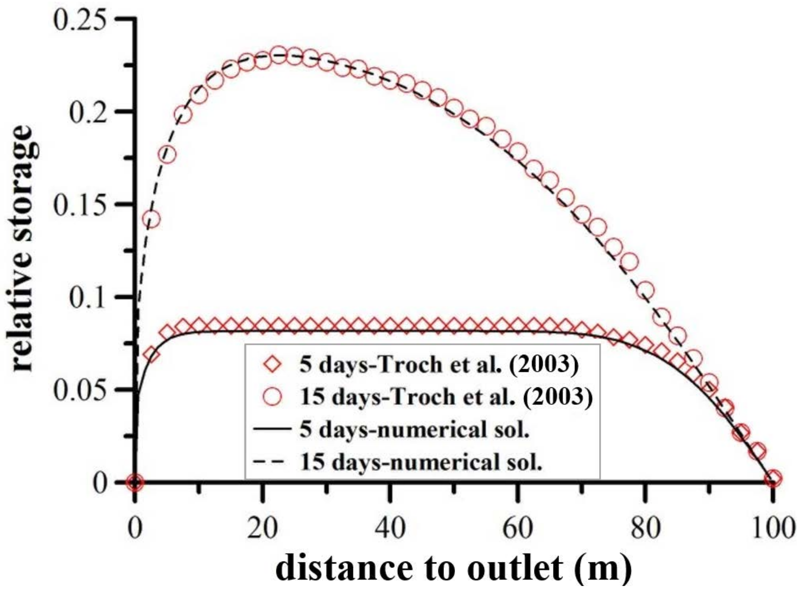

Fig. 6. Comparison of spatial variation of relative storage between the present solutions and previous numerical solutions for $\gamma = 0$, and $R = 10\text{mmd}^{-1}$.

https://doi.org/10.5194/hess-2021-50
Preprint. Discussion started: 23 February 2021

Hydrology and Earth System Sciences
Open Access
Discussions

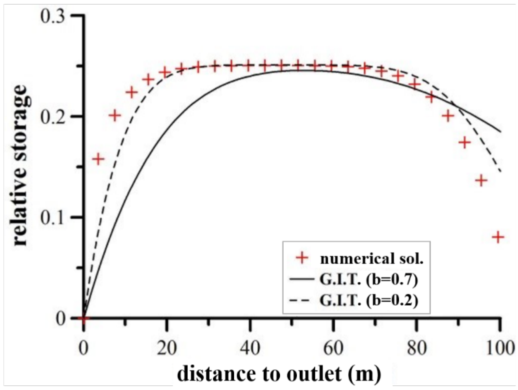

(a) 1day

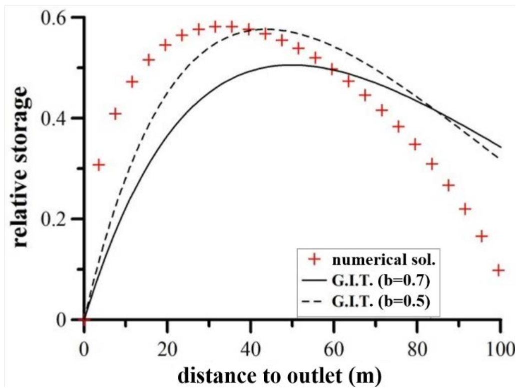

(b) 15 days

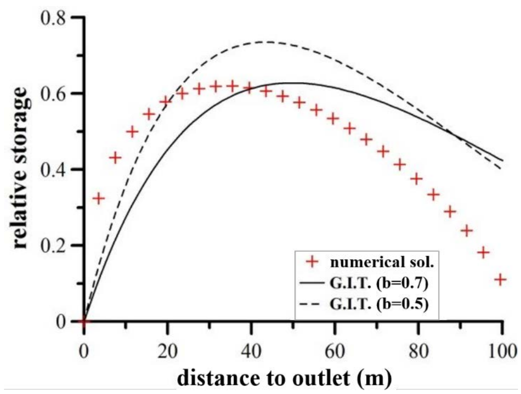

(c) 30 days

Fig. 7. Comparison of relative storage for convergent hillslope between analytical solutions and numerical solutions (R = 50mmd^{-1}).

https://doi.org/10.5194/hess-2021-50
Preprint. Discussion started: 23 February 2021

Hydrology and Earth System Sciences
Open Access
Discussions

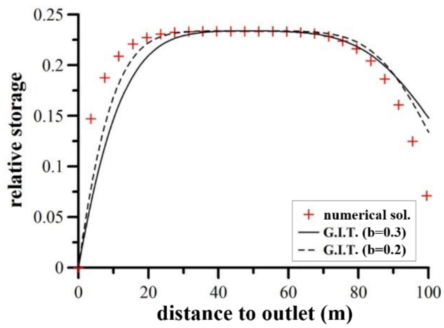

(a) 1 day

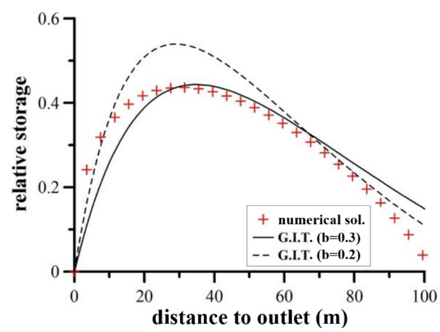

(b) 15 days

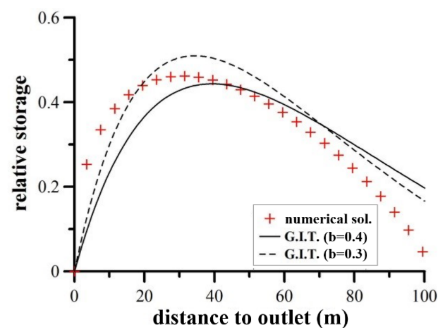

(c) 30 days

Fig. 8. Comparison of relative storage for convergent hillslope between analytical solutions and numerical solutions (R = 25mmd^{-1}).

https://doi.org/10.5194/hess-2021-50
Preprint. Discussion started: 23 February 2021

Hydrology and Earth System Sciences
Discussions

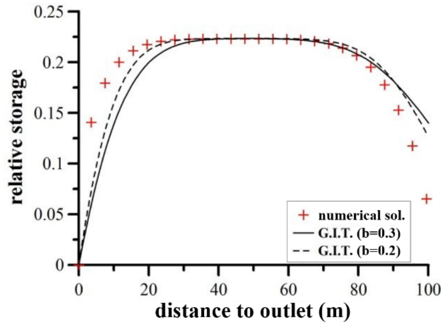

(a) 1 day

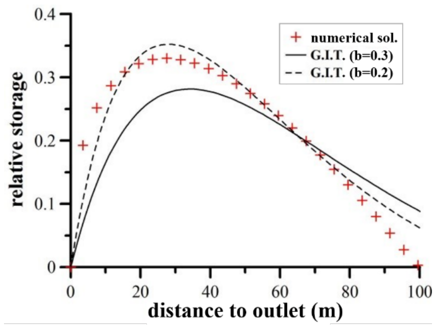

(b) 15 days

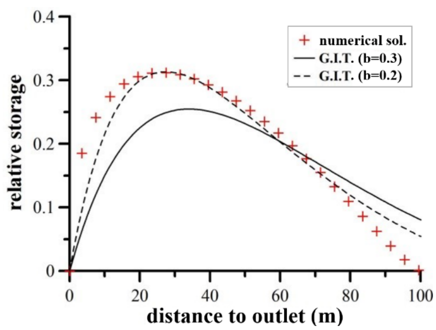

(c) 30 days

Fig. 9. Comparison of relative storage for convergent hillslope between analytical solutions and numerical solutions (R = 10mmd^{-1}).

https://doi.org/10.5194/hess-2021-50
Preprint. Discussion started: 23 February 2021

Hydrology and Earth System Sciences
Open Access
Discussions

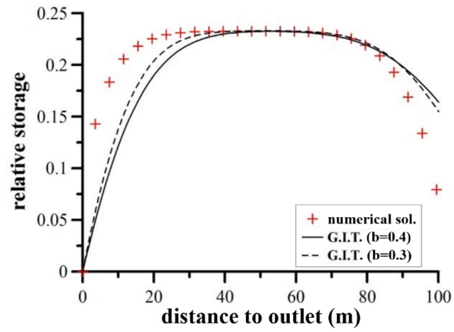

(a) 1 day

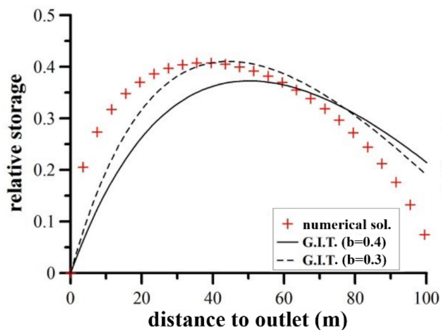

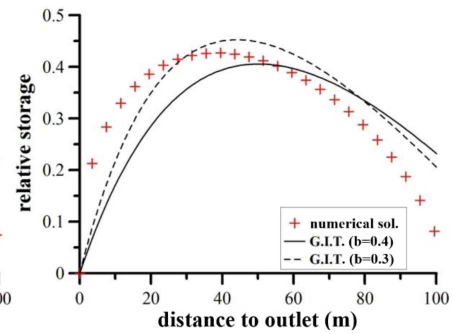

(b) 15 days (c) 30 days

Fig. 10. Comparison of relative storage for uniform hillslope between analytical solutions and numerical solutions (R=50mmd^{-1}, θ=5%).

https://doi.org/10.5194/hess-2021-50
Preprint. Discussion started: 23 February 2021

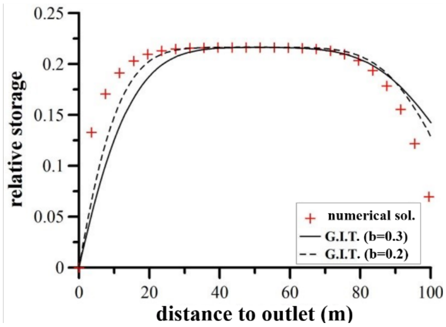

(a) 1 day

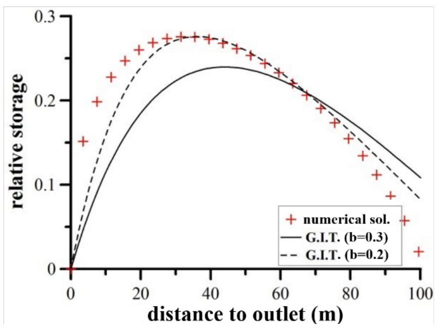

(b) 15 days

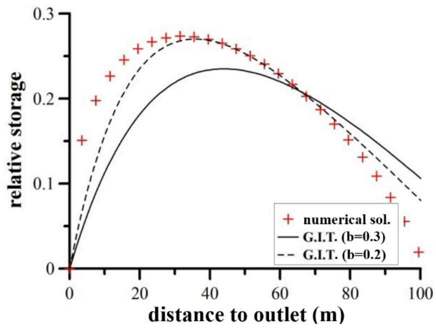

(c) 30 days

Fig. 11. Comparison of relative storage for uniform hillslope between analytical solutions and numerical solutions (R=25mmd^{-1}, θ=5%).

https://doi.org/10.5194/hess-2021-50
Preprint. Discussion started: 23 February 2021

Hydrology and Earth System Sciences
Open Access
Discussions

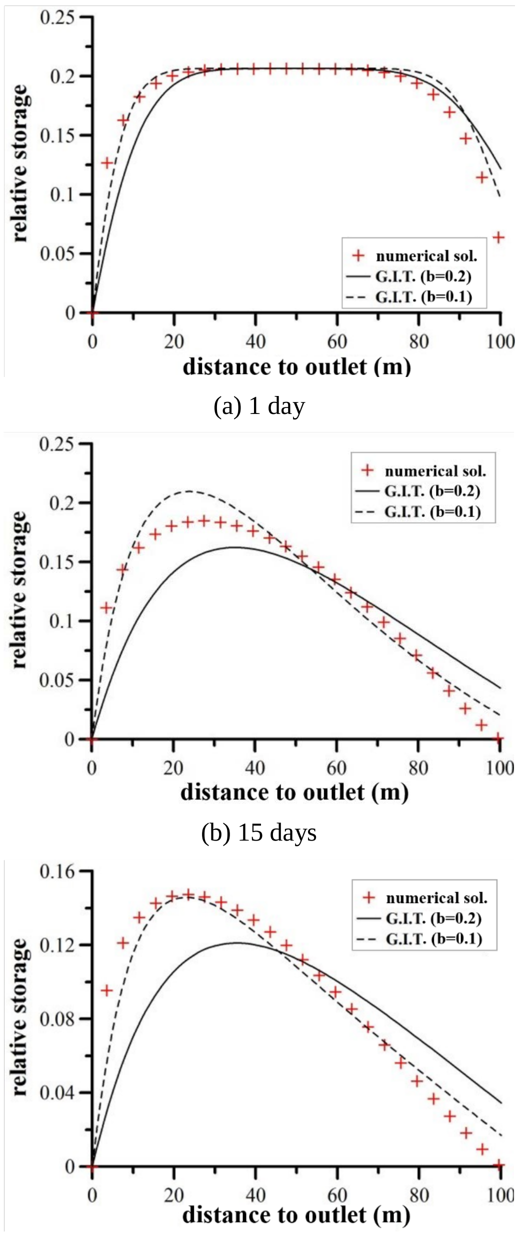

(a) 1 day

(b) 15 days

(c) 30 days

Fig. 12. Comparison of relative storage for uniform hillslope between analytical solutions and numerical solutions (R=10mmd^{-1}, θ=5%).

https://doi.org/10.5194/hess-2021-50
Preprint. Discussion started: 23 February 2021

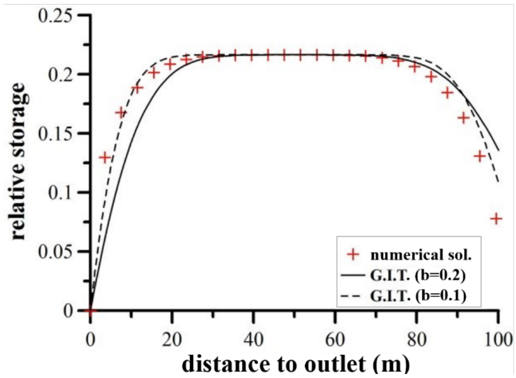

(a) 1day

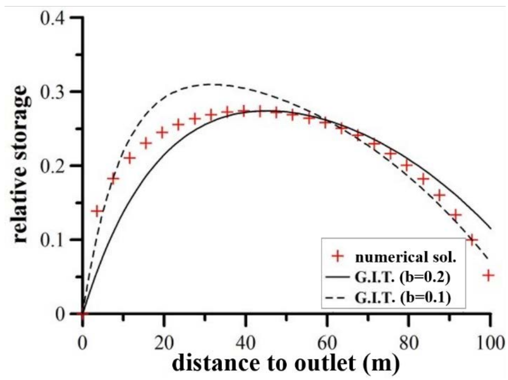

(b) 15days

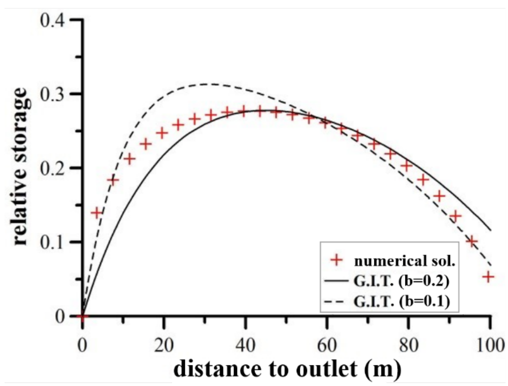

(c) 30days

Fig. 13. Comparison of relative storage for divergent hillslope between analytical solutions and numerical solutions (R=50mmd^{-1}, θ=5%).

https://doi.org/10.5194/hess-2021-50
Preprint. Discussion started: 23 February 2021

Hydrology and Earth System Sciences
Discussions

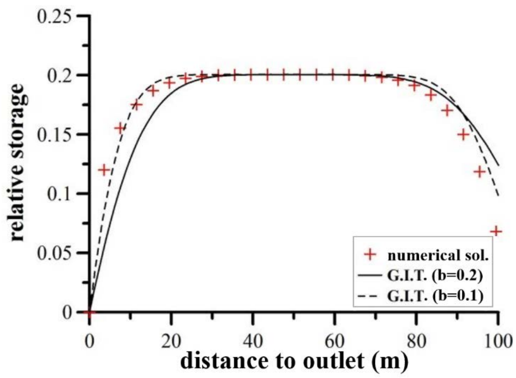

(a) 1day

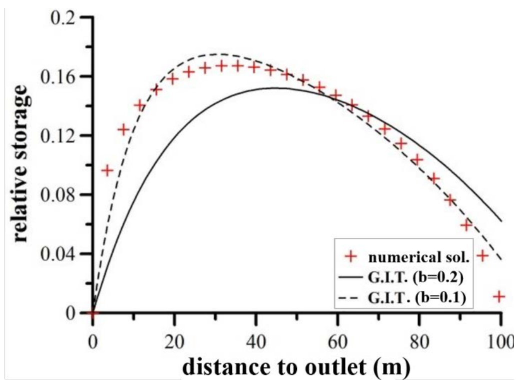

(b) 15days

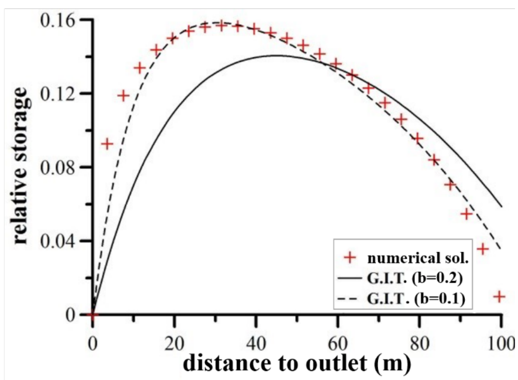

(c) 30days

Fig. 14. Comparison of relative storage for divergent hillslope between analytical solutions and numerical solutions (R=25mmd^{-1}, θ=5%).

Hydrology and Earth System Sciences
Open Access
Discussions

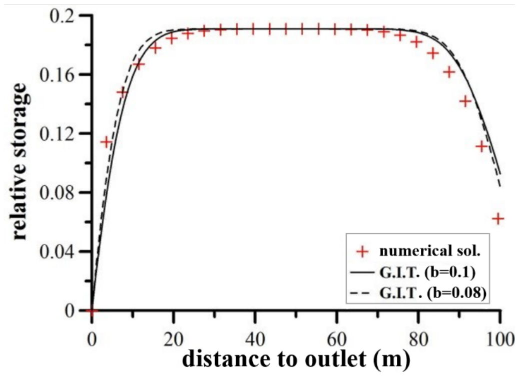

(a) 1day

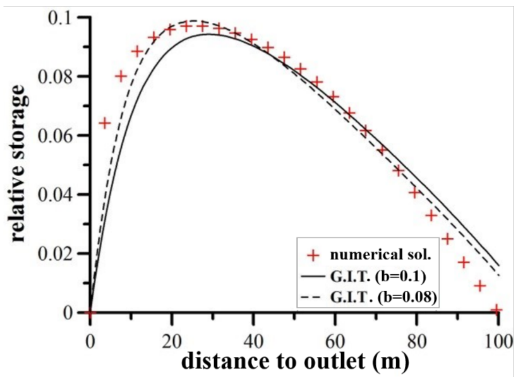

(b) 15days

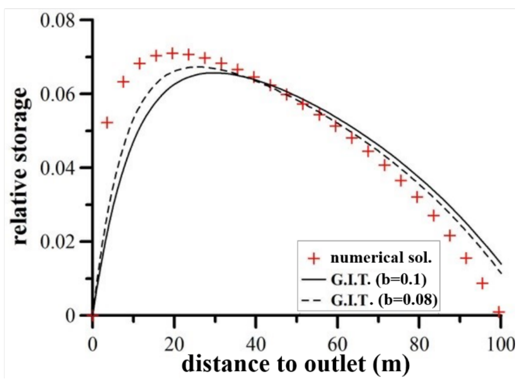

(c) 30days

Fig. 15. Comparison of relative storage for divergent hillslope between analytical solutions and numerical solutions (R=10mmd^{-1}, θ=5%).

https://doi.org/10.5194/hess-2021-50
Preprint. Discussion started: 23 February 2021

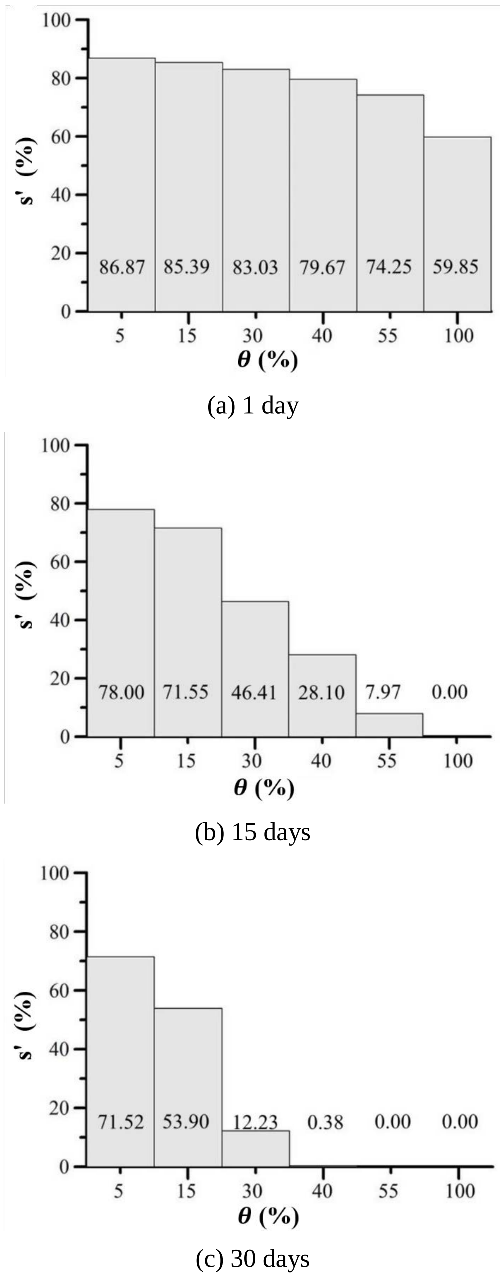

Fig. 16. Variation of the ratio of storage to initial storage at different durations for convergent hillslope.

https://doi.org/10.5194/hess-2021-50
Preprint. Discussion started: 23 February 2021

Hydrology and Earth System Sciences
Open Access
Discussions

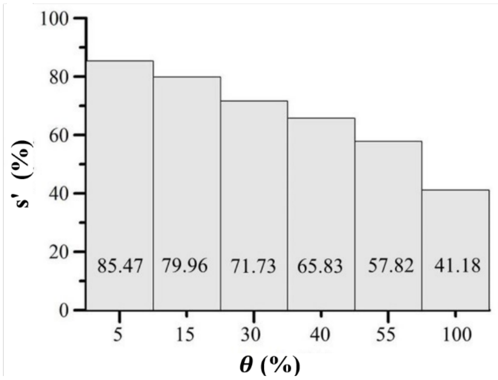

(a) 1 day

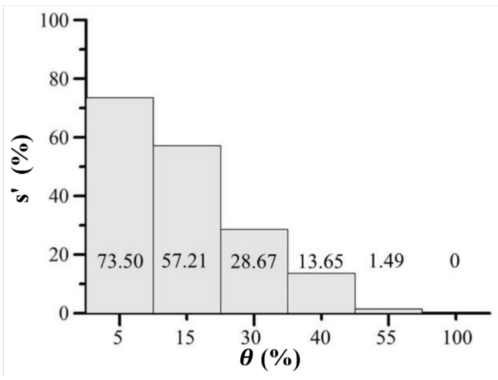

(b) 15 days

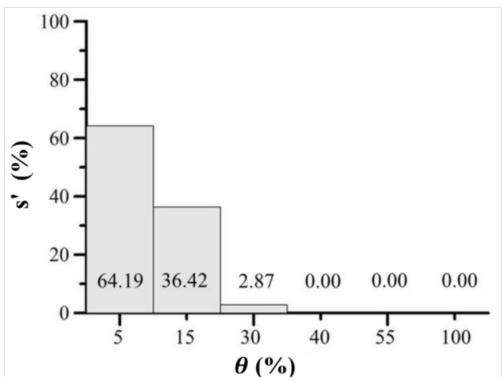

(c) 30 days

Fig. 17. Variation of the ratio of storage to initial storage at different durations for uniform hillslope.

https://doi.org/10.5194/hess-2021-50
Preprint. Discussion started: 23 February 2021

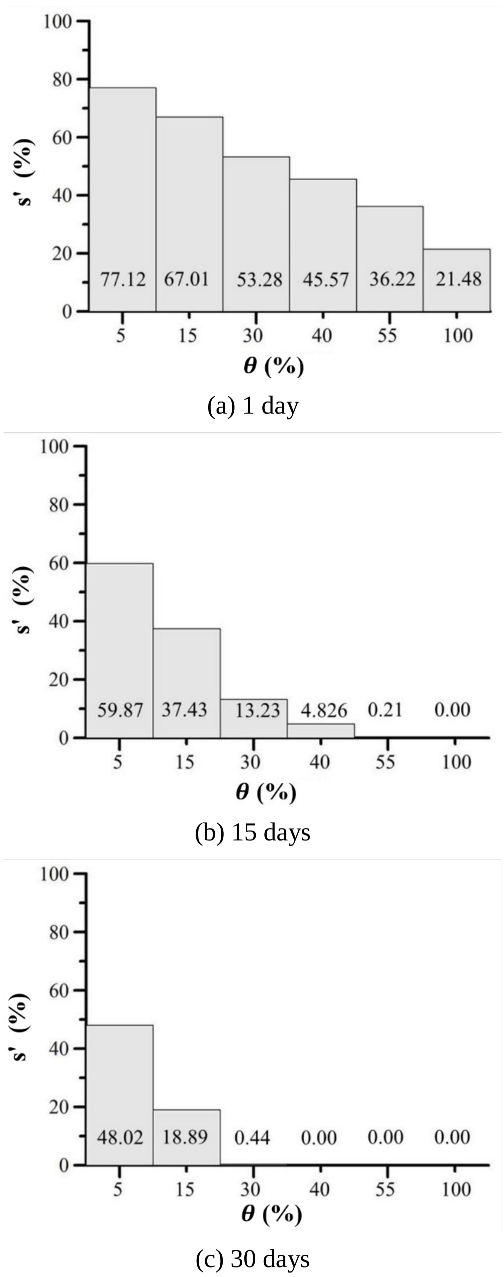

Fig. 18. Variation of the ratio of storage to initial storage at different durations for divergent hillslope.

https://doi.org/10.5194/hess-2021-50
Preprint. Discussion started: 23 February 2021

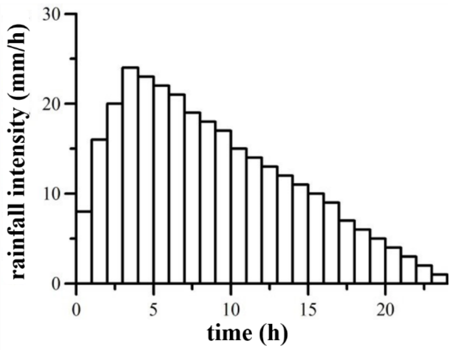

(a) peak at the first quarter section

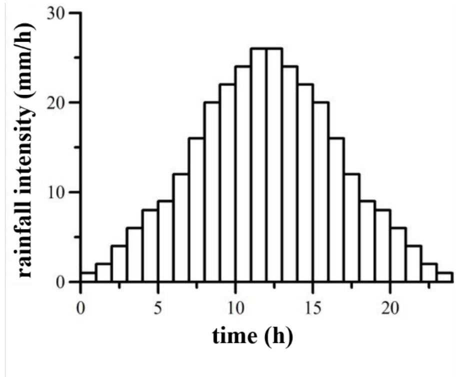

(b) peak at center

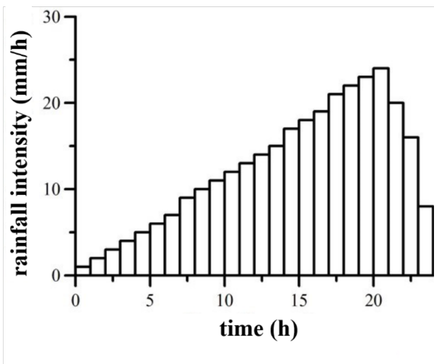

(c) peak at the third quarter section

Fig. 19. Presumed patterns of temporally various distributed recharge rates.

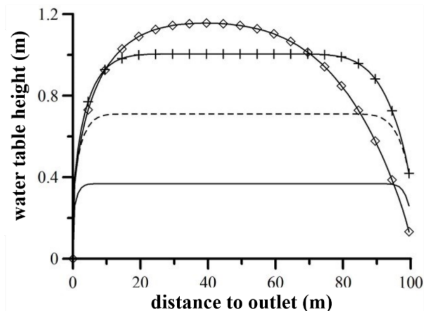

(a) peak at the first quarter section

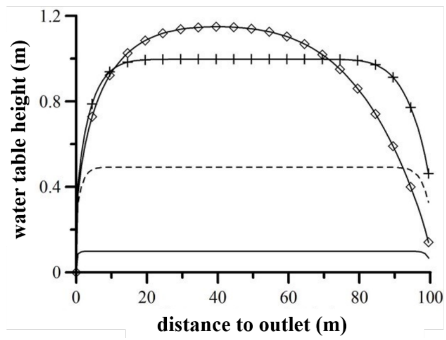

(b) peak at center

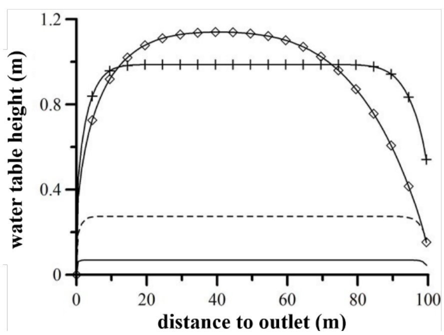

(c) peak at the third quarter section

6 hours 12 hours 24 hours 72 hours

Fig. 20. Variation of water table for three patterns of recharge distribution for convergent hillslope.

https://doi.org/10.5194/hess-2021-50
Preprint. Discussion started: 23 February 2021

Hydrology and Earth System Sciences
Open Access
Discussions

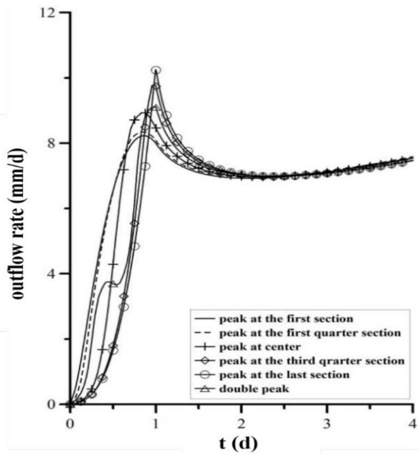

(a) convergent hillslope

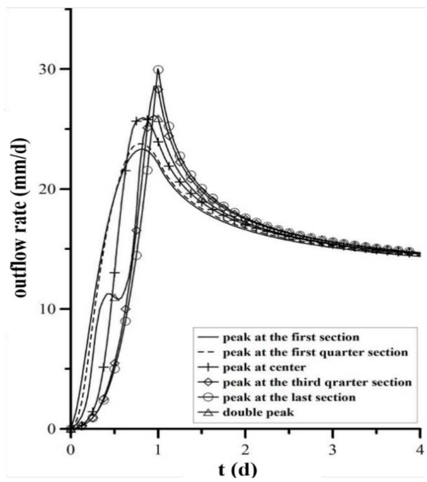

(b) uniform hillslope

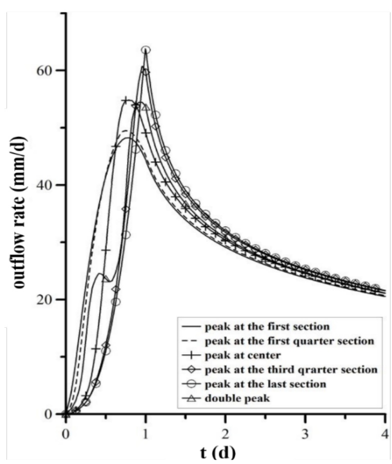

(c) divergent hillslope

Fig. 21. Hydrograph of outflow for three different hillslopes under six types of recharge distribution.